Ultra-broadband asymmetric acoustic transmission with single transmitted beam*

Ding Jia(贾鼎)[1], Hong-xiang Sun(孙宏祥)[1,2,†], Shou-qi Yuan(袁寿其)[1,‡], and Yong Ge(葛勇)[1]

[1] *Research Center of Fluid Machinery Engineering and Technology, Faculty of Science, Jiangsu University, Zhenjiang* 212013, *China*
[2] *State Key Laboratory of Acoustics, Institute of Acoustics, Chinese Academy of Sciences, Beijing* 100190, *China*

(Received 9 October 2016; revised manuscript received 15 November 2016; published online 20 December 2016)

We report both experimentally and numerically that ultra-broadband asymmetric acoustic transmission is realized by a brass plate and a right triangle reflector immersed in water. This exotic phenomenon arises from the asymmetric excitation of the leaky asymmetric zero-order Lamb mode in the brass plate induced by the incident angle of external bulk waves. The results show that the bandwidth of the asymmetric acoustic transmission could reach 2000 kHz, and the positive transmitted wave is only a single acoustic beam. The device has the advantages of ultra-broadband, single transmitted beam, and simpler structure, which has great potential applications in ultrasonic devices.

Keywords: asymmetric acoustic transmission, acoustic wave, plate, Lamb mode

PACS: 43.35.+d, 43.20.+g **DOI:** 10.1088/1674-1056/26/2/024302

1. Introduction

Acoustic analogies of electrical diodes, which have the exotic property of allowing acoustic waves to transmit through one direction as well as blocking the transmission along the opposite direction, have recently attracted rapidly growing interest in the fields of physics and medicine owing to their great potential applications in many practical scenarios. For example, the elimination of the reflected wave energy may help to improve the quality of medical ultrasound imaging, and enable the design of conceptual devices like unidirectional sound barriers for noise control. The rapid development of sonic crystals and acoustic metamaterials provides various acoustic properties unavailable in nature,[1–7] enabling the design of various acoustic one-way devices.

Recently, many mechanisms have been proposed for designing various acoustic one-way devices by breaking the time reversal symmetry with nonlinear media,[8–10] active methods,[11–13] or gain-loss pair.[14–18] Due to the intrinsic limitations of nonlinear effects, including the inherent signal distortions and transmission efficiency, etc., more attentions have been focused on the asymmetric acoustic transmission (AAT). Several linear acoustic devices have been proposed to realize the AAT, such as acoustic gratings,[19–25] phononic crystals,[26–30] metamaterials,[31,32] and metasurfaces,[33–35] which have advantages of the high transmission efficiency and broad bandwidth of the AAT. However, for most of these AAT structures, the positive transmitted waves are usually two beam,[22] three beam,[19,20] multiple beam,[23,24,26] or distorted waveform in waveguides,[28–30,34,35] and it is difficult to concentrate the transmitted energy into a signal acoustic beam. In this context, the AAT effect with a single transmitted beam has been obtained based on the asymmetric phase modulation.[32,33] But the bandwidth of the AAT is limited owing to the coupling of a gradient-index metasurface and a near-zero-index medium, and it is still a challenge to realize the broadband AAT effect with a single transmitted beam. This restriction apparently becomes an obstacle for the practical application of the AAT.

In this work, we propose a simple acoustic device for realizing the ultra-broadband AAT effect with a single transmitted beam, which consists of a brass plate and a right triangle reflector in water. In the AAT device, the working bandwidth could reach 2000 kHz with the incident angle of 48°, and the positive transmitted wave is only a single acoustic beam. The experimental results agree well with the numerical simulations. Moreover, the AAT effect with different incident angles and plate thicknesses are investigated in detail.

2. Experimental and numerical models

As schematically shown in Fig. 1, the AAT device under consideration is a brass plate and a right triangle reflector immersed in water. The abbreviations TI and BI refer to the acoustic waves normally incident from the top and bottom sides of the AAT device, respectively. For TI, the incident

*Project supported by the Major Program of the National Natural Science Foundation of China (Grant No. 51239005), the National Natural Science Foundation of China (Grant No. 11404147), the Natural Science Foundation of Jiangsu Province of China (Grant No. BK20140519), China Postdoctoral Science Foundation (Grant No. 2015M571672), the Scientific Research Project for Graduate Students of Universities in Jiangsu Province, China (Grant No. CXZZ13_06), and the Training Project of Young Backbone Teachers of Jiangsu University.

†Corresponding author. E-mail: jsdxshx@ujs.edu.cn
‡Corresponding author. E-mail: Shouqiy@ujs.edu.cn

© 2017 Chinese Physical Society and IOP Publishing Ltd

wave is firstly reflected by the triangle reflector, and arrives at the brass plate with an incident angle, and the relationship between the incident angle α and the base angle θ is $\alpha = 180°–2\theta$. However, for BI, the incident wave is incident on the brass plate vertically, and the parameter α is 0°. Throughout this work, the finite element method based on COMSOL Multiphysics software is utilized to numerically calculate the AAT characteristics. The structure parameters are $d = 3.0$ mm, $l = 30.0$ mm, and $h = 1.0$ mm, and the material parameters are adopted as follows: the density $\rho = 8400$ kg/m^3, the longitudinal wave velocity $c_l = 4400$ m/s, and the transversal wave velocity $c_t = 2200$ m/s for brass; $\rho_w = 998$ kg/m^3, $c_w = 1483$ m/s for water, at the temperature 296 K. In addition, the width of the incident plane wave is 20 mm.

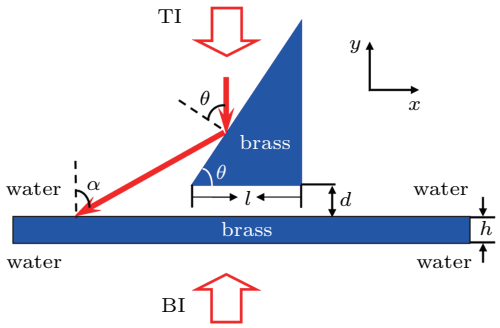


Fig. 1. (color online) Schematic diagram of AAT device.

3. Properties of AAT

3.1. Transmission spectra

Figures 2(a)–2(c) show the numerical transmittance spectra for TI and BI. The base angle θ is 58°, 60°, and 62° which correspond to the parameter α: 64°, 60°, and 56°, respectively. The AAT effect exists in the ranges 428 kHz–901 kHz, 547 kHz–1038 kHz, and 720 kHz–1267 kHz for $\alpha = 64°$, 60°, and 56°, respectively, which are plotted in the black shaded regions. The maximum bandwidth of the AAT reaches about 550 kHz for $\alpha = 56°$, which is much wider than previous broadband AAT devices.[22,23,28,29] Besides, the peaks of the transmittance spectra for TI locate at 693 kHz, 819 kHz, and 1018 kHz for $\alpha = 64°$, 60°, and 56°, respectively. It indicates that, with the decrease of α, the working band of the AAT becomes much wider and moves to the high frequency region.

To quantify the AAT performance, we introduce the contrast ratio (δ) as $\delta = |T_T - T_B|/(T_T + T_B)$, where T_T and T_B are the transmittances for TI and BI, respectively. Figures 2(d)–2(f) present the contrast ratio with different α which correspond to Figs. 2(a)–2(c), respectively. In the black shaded regions, most values of δ are close to 1.0 in the working bands of the AAT, indicating that the AAT devices have good performance.

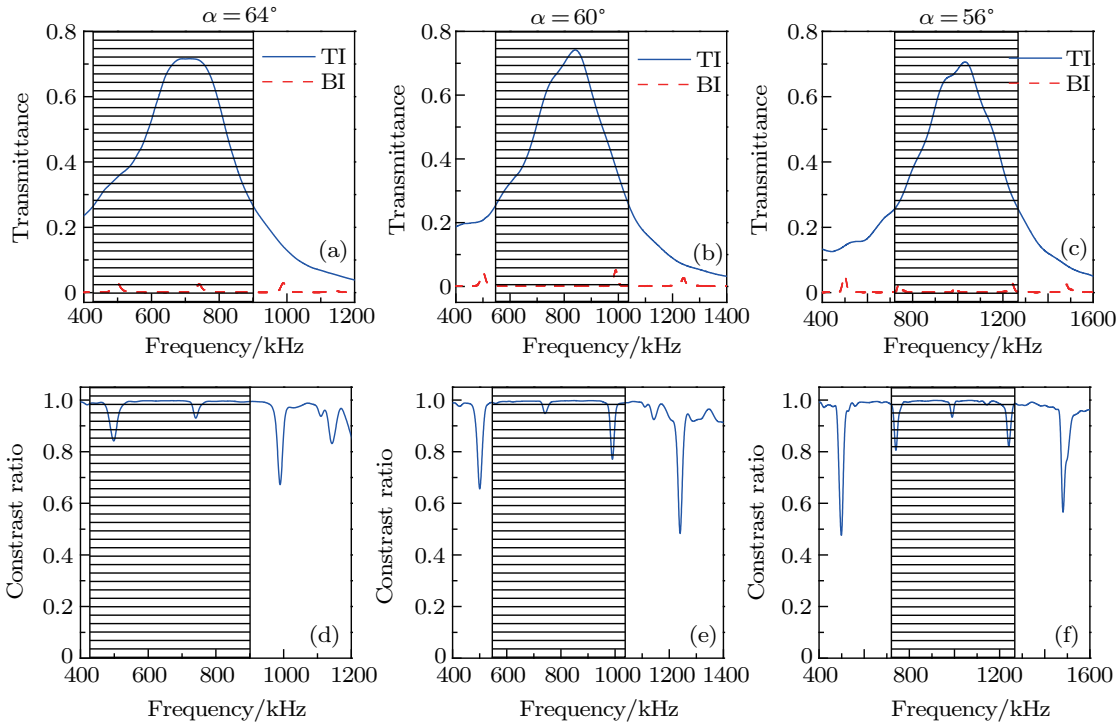


Fig. 2. (color online) Numerical transmittance spectra for (a) $\alpha = 64°$, (b) $\alpha = 60°$, and (c) $\alpha = 56°$, and numerical contrast ratio for (d) $\alpha = 64°$, (e) $\alpha = 60°$, and (f) $\alpha = 56°$.

Figure 3 shows the spatial distributions of the intensity field through the AAT devices. The incident frequencies are 693 kHz for $\alpha = 64°$ [Figs. 3(a) and 3(b)], 819 kHz for $\alpha = 60°$ [Figs. 3(c) and 3(d)], and 1018 kHz for $\alpha = 56°$ [Figs. 3(e) and 3(f)], respectively. In the case of TI [Figs. 3(a), 3(c), and 3(e)], the incident wave is firstly reflected by the triangle reflector, and reaches the brass plate with an incident angle α, and finally transmits through the brass plate, form-

ing only a single acoustic beam. However, in the case of BI [Figs. 3(b), 3(d), and 3(f)], the incident angle α is 0°, and the acoustic wave is almost completely reflected without any transmission.

3.2. Physical mechanism of AAT

Figures 3(g)–3(i) present the zoom of the deformation of the displacement field in the brass plate in Figs. 3(a), 3(c), and 3(e), respectively. Note that the asymmetric zero-order Lamb wave (A_0 mode) is excited for TI. In general, if the phase velocity of the Lamb wave in the brass plate is larger than the bulk velocity in water, the Lamb wave could couple energy into water, creating a leaky bulk wave at a critical angle. The leakage angle (θ) is defined as $\theta = \sin^{-1}(c_w/c_p)$, where c_w is the bulk velocity of the water, and c_p is the phase velocity of the Lamb wave.[36,37]

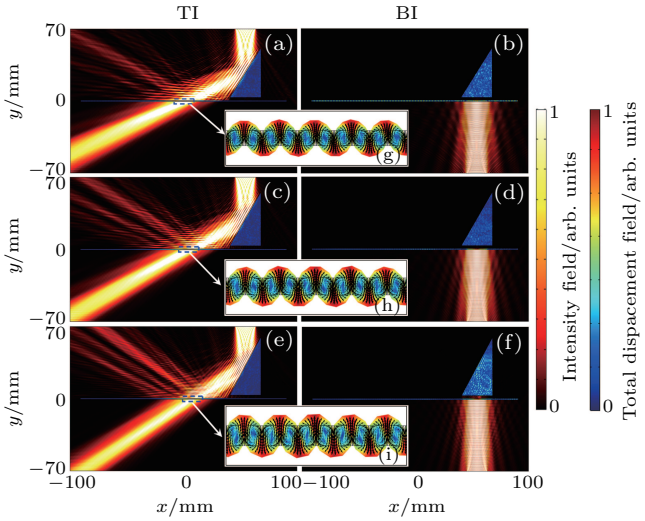


Fig. 3. (color online) Numerical acoustic intensity field for (a) and (b) $\alpha = 64°$ at 693 kHz, (c) and (d) $\alpha = 60°$ at 819 kHz, (e) and (f) $\alpha = 56°$ at 1018 kHz, deformation of displacement field in brass plate for TI at (g) 693 kHz, (h) 819 kHz, and (i) 1018 kHz, and black arrows represent vibration directions of displacements.

Figure 4 shows the leaky angle distribution of the A_0 mode, in which the frequencies at points *A*, *B*, and *C* are 693 kHz, 819 kHz, and 1018 kHz, corresponding to the leaky angles of the A_0 mode 64°, 60°, and 56°, respectively. These frequencies and angles are the same as those in Figs. 3(a), 3(c), and 3(e). Besides, the A_0 mode in the brass plate could be excited when the incident angle of the external bulk wave is the same as or close to the leaky angle at a certain frequency.[38] Therefore, the acoustic wave can pass through the brass plate, which is shown in Figs. 3(a), 3(c), and 3(e). However, in Figs. 3(b), 3(d), and 3(f), the incident angle has great difference with the leaky angle, so little energy could transmit through the brass plate. Furthermore, as shown in Fig. 4, the gradient of the leaky angle curve of the A_0 mode at point *C* is smaller than that at points *A* and *B*, which explains that the working band of the AAT becomes much wider with the decrease of α. It is deduced that the AAT effect is attributed to the asymmetric excitation of the A_0 mode in the brass plate induced by the incident angle of the external bulk wave, and the band of the AAT is determined by the incident angle and its corresponding gradient of the leaky angle curve.

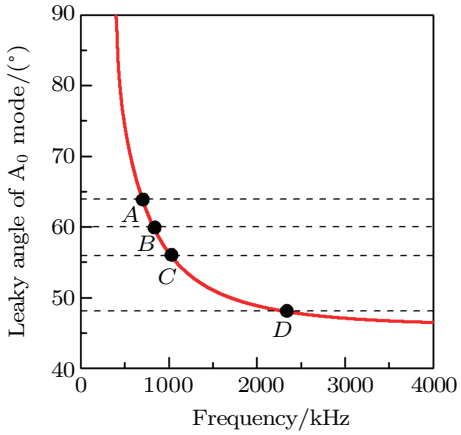


Fig. 4. (color online) Leaky angle distribution of A_0 mode in brass plate with thickness of 1.0 mm in water.

3.3. Experimental verifications

In order to experimentally verify the AAT effect, we have measured acoustic transmittances by the well-known ultrasonic transmission technique.[39] In the AAT models, the right triangle reflector is used to adjust the incident direction of acoustic waves for TI, and is replaced by a rotating ultrasonic transducer in the experiment. Figure 5 shows the schematic diagram of the experimental setup. The brass plate with the thickness of 1.0 mm is placed between two broadband ultrasonic transducers, one as generator and the other as detector, which is immersed in a water tank. Owing to the bandwidth limitation, two pairs of ultrasonic transducers (diameters of 20 mm) are used to fully cover the working range of the AAT from 300 kHz to 1500 kHz. One pair works at 500-kHz central frequency and 250 kHz–1100 kHz bandwidth, and the other pair at 1000-kHz central frequency and 700 kHz–1600 kHz bandwidth. The generation and detection transducers are obliquely towards the center of the brass plate with the same distance of 10 cm, and the incident angle of the generation transducer are set as 64°, 60°, and 56° which correspond to the incident angle α for TI in Figs. 2(a)–2(c), respectively. Besides, the incident angle of 0° is also measured, corresponding to that for BI.

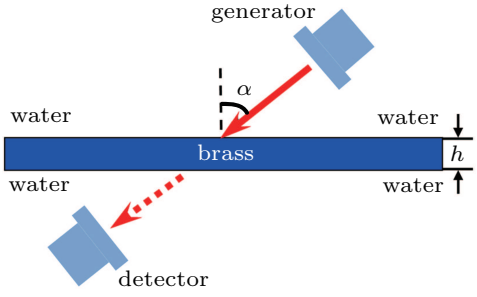


Fig. 5. (color online) Schematic diagram of experimental setup.

Figure 6 shows the measured transmittance spectra of different incident angles, in which the corresponding numerical results are plotted for comparison. The measured transmittance spectra agree with the numerical results. Moreover, as shown in the black shaded regions, the characteristics of the transmittance spectra agree well with those in the band of the AAT in Figs. 2(a)–2(c), which verifies the feasibility of the AAT device.

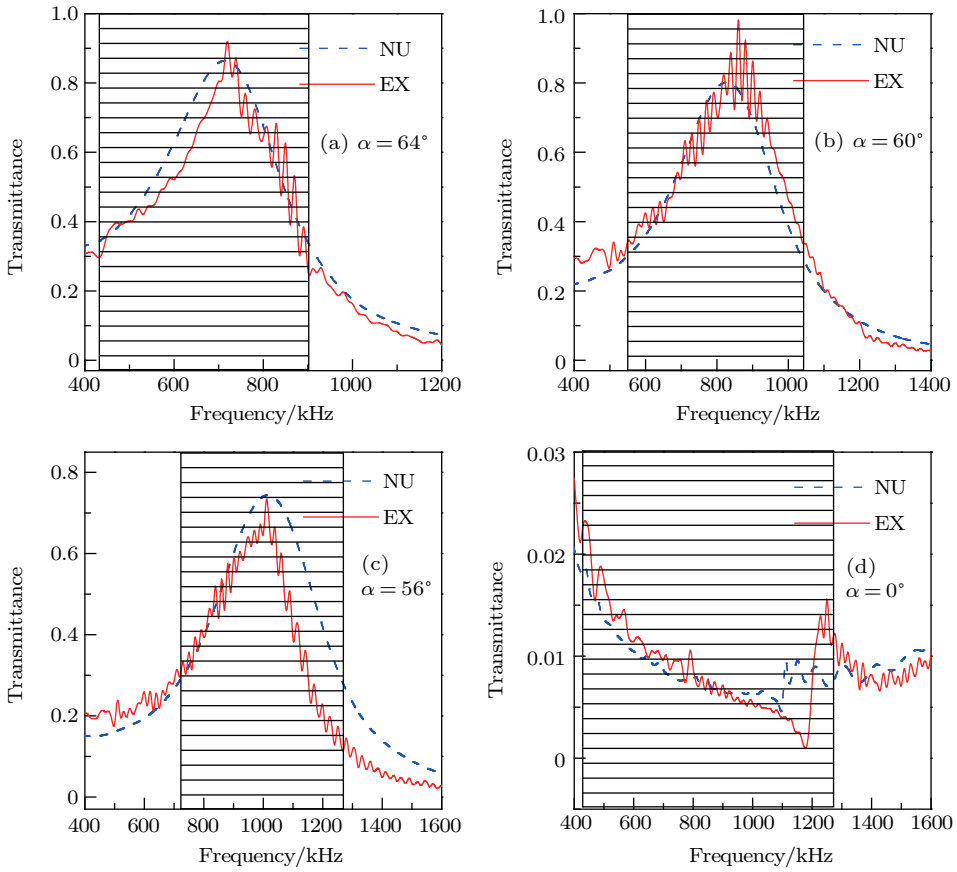


Fig. 6. (color online) Numerical (NU) and experimental (EX) transmittance spectra for (a) $\alpha = 64°$, (b) $\alpha = 60°$, (c) $\alpha = 56°$, and (d) $\alpha = 0°$.

3.4. Ultra-broadband AAT

According to this mechanism of the AAT, we could realize the ultra-broadband AAT effect with the single transmitted beam by the excitation of the external bulk waves with the incident angle α of 48°. Figures 7(a) and 7(b) show the numerical transmittance spectra and contrast ratio, respectively, in which the base angle θ is 66°. Note that the working band of the AAT is in the range 1320 kHz–3320 kHz (black shaded region) and is up to 2000 kHz with the incident angle of 48°. Besides, the maximum transmittance for TI is about 0.65 at 2320 kHz, whereas the transmittance for TI is close to zero. Furthermore, as shown in Fig. 7(b), most values of δ are close to 1.0 in the black shaded region, indicating that the device has good performance in this ultra-broad band of the AAT.

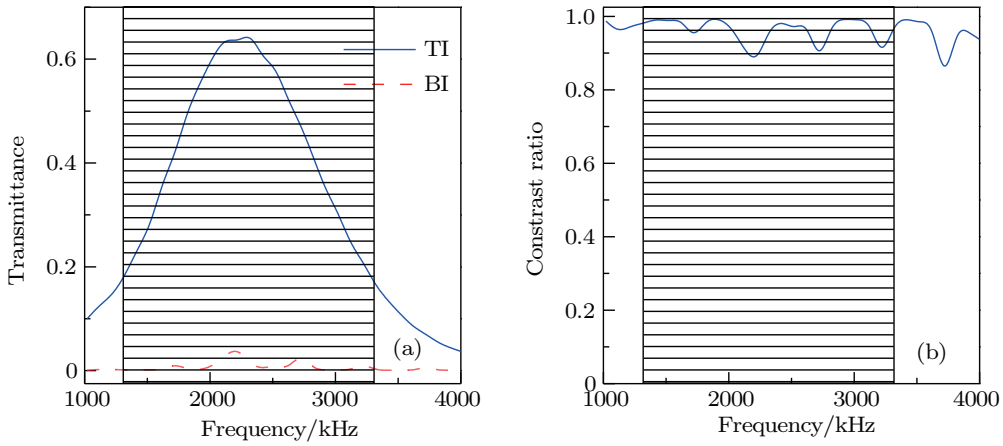


Fig. 7. (color online) Numerical (a) transmittance spectra and (b) contrast ratio for $\alpha = 48°$.

As shown in Fig. 4, the frequency and the leaky angle at point D are 2320 kHz and 48°. The leaky angle, the A_0 mode and the frequency at point D are the same as the incident angle and the frequency of the maximum transmittance for TI in Fig. 7(a). Therefore, the ultra-broadband AAT effect arises from the excitation of the A_0 mode. Besides, the gradient of the leaky angle curve of the A_0 mode at point D is much smaller than that at points A, B, and C. Therefore, the working band of the AAT can reach 2000 kHz, which is much wider than previous broadband AAT devices.

3.5. Different plate thickness

Figures 8(a) and 8(b) show the numerical transmittance spectra with the plate thickness (h) of 0.8 mm and 1.2 mm. In the simulations, the parameters are the same as those in Fig. 2(c), and incident angle α for TI is 56°. It is shown from Figs. 8(a) and 8(b) that the working bands of the AAT are 895 kHz–1600 kHz and 585 kHz–1068 kHz, respectively. Note that, with the increase of h, the band of the AAT becomes narrower and moves to the low frequency region.

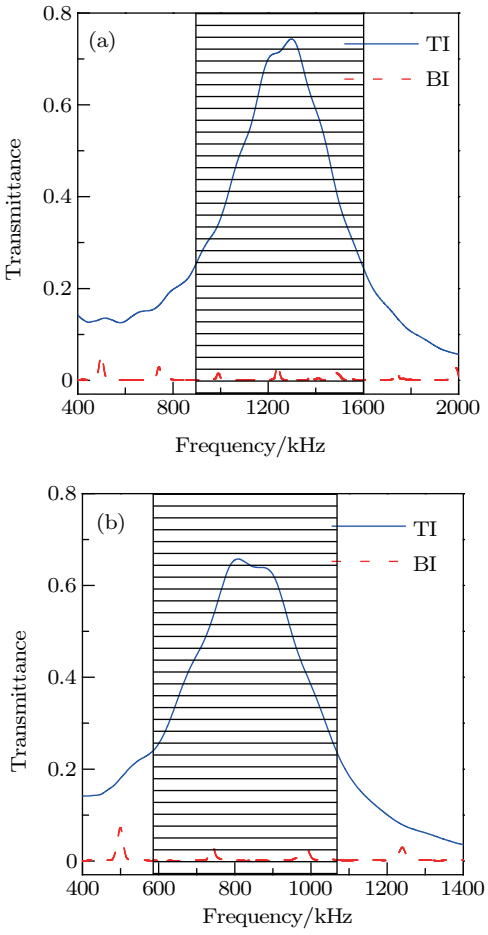


Fig. 8. (color online) Numerical transmittance spectra for (a) $h =$ 0.8 mm and (b) $h = 1.2$ mm.

Figure 9 displays the leaky angle curve of the A_0 mode in the brass plate with the thickness of 0.8 mm and 1.2 mm, in which the leaky angle of both points E and F is 56°. With the increase of h, the leaky angle curve of the A_0 mode shifts to the low frequency region, and thus the frequencies at points E and F are 800 kHz and 1200 kHz, respectively. Besides, the AAT effect exists only when the incident angle of the external bulk wave is the same as or close to the leaky angle of the A_0 mode. Therefore, the bands of the AAT are 895 kHz–1600 kHz and 585 kHz–1068 kHz for $h = 0.8$ mm and 1.2 mm, respectively. Furthermore, the gradient of the leaky angle curves of the A_0 mode at point F is smaller than that at point E, and this explains that the band of the AAT becomes narrower with the increase of h. In addition to the incident angle, the band of the AAT is also closely related to the plate thickness.

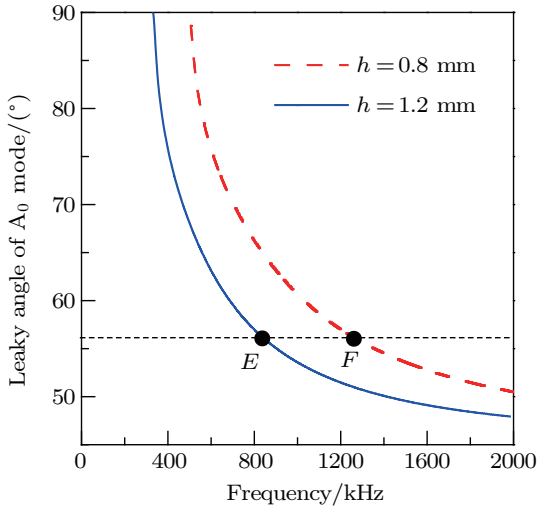


Fig. 9. (color online) Leaky angle distribution of A_0 mode in brass plate with thickness of 0.8 mm and 1.2 mm in water.

3.6. Two positive transmitted waves

We also find that the transmitted waves could be divided into two beams by using an isosceles triangle reflector, which is schematically shown in Fig. 10. The structure parameters are $\theta = 62°$, $d = 3.0$ mm, $l = 30.0$ mm, and $h = 1.0$ mm. Figure 11 shows the spatial distributions of the intensity field through the device with the incident frequency of 1018 kHz. For TI [Fig. 11(a)], the incident wave is divided into two beams by the isosceles triangle reflector, and reaches the brass plate with an incident angle (α) of 56°, and transmits through the brass plate with two beams. However, in the case of BI [Fig. 11(b)], the acoustic energy is also completely reflected.

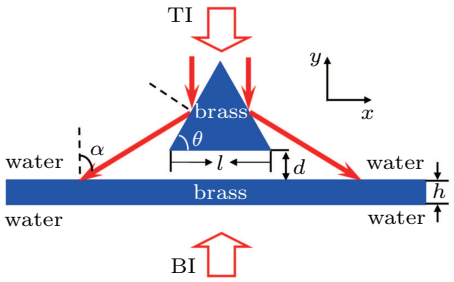


Fig. 10. (color online) Schematic diagram of AAT device with isosceles triangle reflector.

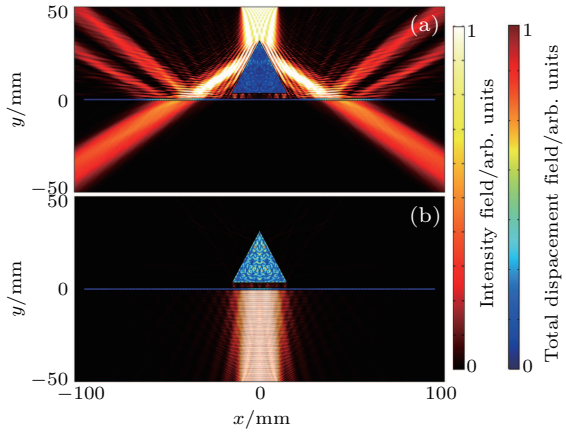


Fig. 11. (color online) Numerical acoustic intensity field with isosceles triangle reflector for (a) TI and (b) BI at 1018 kHz.

4. Conclusions

In conclusion, using a new type of structure, we have demonstrated the ultra-broadband AAT both experimentally and numerically. The ultra-broadband AAT effect is attributed to the asymmetric excitation of the leaky A_0 mode in the brass plate induced by the incident angle of external bulk waves. The results show that the bandwidth of the AAT could reach 2000 kHz with the incident angle of 48°, and the positive transmitted wave is only a single beam. Besides, the band of the AAT is closely related to the incident angle, gradient of the leaky angle curve, and plate thickness. The measured transmittances agree well with the numerical simulations. The results have important scientific significances and potential applications in ultra-broadband unidirectional acoustic devices with a single transmitted beam.

References

[1] Liu Z Y, Zhang X X, Mao Y W, Zhu Y Y, Yang Z Y, Chan C T and Sheng P 2000 *Science* **289** 1734

[2] Fang N, Xi D, Xu J, Ambati M, Srituravanich W, Sun C and Zhang X 2006 *Nat. Mater.* **5** 452

[3] Lu M H, Zhang C, Feng L, Zhao J, Chen Y F, Mao Y W, Zi J, Zhu Y Y, Zhu S N and Ming N B 2007 *Nat. Mater.* **6** 744

[4] Cheng Y, Zhou C, Yuan B G, Wu D J, Wei Q and Liu X J 2015 *Nat. Mater.* **14** 1013

[5] Xiao M, Ma G C, Yang Z Y, Sheng P, Zhang Z Q and Chan C T 2015 *Nat. Phys.* **11** 240

[6] Xu C Q, Fang A A, Chu H C, Luo J, Chan C T, Hang Z H and Lai Y 2016 *Phys. Rev. B* **93** 245116

[7] Guan Y J, Sun H X, Liu S S, Yuan S Q, Xia J P and Ge Y 2016 *Chin. Phys. B* **25** 104302

[8] Liang B, Yuan B and Cheng J C 2009 *Phys. Rev. Lett.* **103** 104301

[9] Liang B, Yuan Y and Cheng J C 2015 *Acta Phys. Sin.* **64** 094305 (in Chinese)

[10] Boechler N, Theocharis G and Daraio C 2011 *Nat. Mater.* **10** 665

[11] Fleury R, Sounas D L, Sieck C F, Haberman M R and Alù A 2014 *Science* **343** 516

[12] Popa B I and Cummer S A 2014 *Nat. Commun.* **5** 3398

[13] Ni X, He C, Sun X C, Liu X P, Lu M H, Feng L and Chen Y F 2015 *New J. Phys.* **17** 053016

[14] Zhu X F, Ramezani H, Shi C Z, Zhu J and Zhang X 2014 *Phys. Rev. X* **4** 031042

[15] Fleury R, Sounas D and Alù A 2015 *Nat. Commun.* **6** 5905

[16] Liu C, Du Z L, Sun Z, Gao H J and Guo X 2015 *Phys. Rev. Appl.* **3** 064014

[17] Shi C Z, Dubois M, Chen Y, Cheng L, Ramezani H, Wang Y and Zhang X 2016 *Nat. Commun.* **7** 11110

[18] Gu Z M, Hu J, Liang B, Zou X Y and Cheng J C 2016 *Sci. Rep.* **6** 19824

[19] He Z J, Peng S S, Ye Y T, Dai Z W, Qiu C Y, Ke M Z and Liu Z Y 2011 *Appl. Phys. Lett.* **98** 083505

[20] Sun H X, Zhang S Y and Shui X J 2012 *Appl. Phys. Lett.* **100** 103507

[21] Jia H, Ke M Z, Li C H, Qiu C Y and Liu Z Y 2013 *Appl. Phys. Lett.* **102** 153508

[22] Sun H X and Zhang S Y 2013 *Appl. Phys. Lett.* **102** 113511

[23] Li C H, Ke M Z, Ye Y T, Xu S J, Qiu C Y and Liu Z Y 2014 *Appl. Phys. Lett.* **105** 023511

[24] Sun H X, Yuan S Q and Zhang S Y 2015 *Appl. Phys. Lett.* **107** 213505

[25] Zhang S, Zhang Y, Guo Y J, Leng Y H, Feng W and Cao W W 2016 *Phys. Rev. Appl.* **5** 034006

[26] Li X F, Ni X, Feng L, Lu M H, He C and Chen Y F 2011 *Phys. Rev. Lett.* **106** 084301

[27] Cicek A, Kaya O A and Ulug B 2012 *Appl. Phys. Lett.* **100** 111905

[28] Yuan B, Liang B, Tao J C, Zou X Y and Cheng J C 2012 *Appl. Phys. Lett.* **101** 043503

[29] Huang Y L, Sun H X, Xia J P, Yuan S Q and Ding X L 2016 *Appl. Phys. Lett.* **109** 013501

[30] Ouyang S L, He H L, He Z J, Deng K and Zhao H P 2016 *J. Appl. Phys.* **120** 104504

[31] Li Y, Liang B, Gu Z, Zou X and Cheng J C 2013 *Appl. Phys. Lett.* **103** 053505

[32] Shen C, Xie Y B, Li J F, Cummer S A and Jing Y 2016 *Appl. Phys. Lett.* **108** 223502

[33] Jiang X, Liang B, Zou X Y, Yang J, Yin L L, Yang J and Cheng J C 2016 *Sci. Rep.* **6** 28023

[34] Zhu Y F, Zou X Y, Liang B and Cheng J C 2015 *Appl. Phys. Lett.* **106** 173508

[35] Wang X P, Wan L L, Chen T N, Liang Q X and Song A L 2016 *Appl. Phys. Lett.* **109** 044102

[36] Sun H X, Zhang S Y, Yuan S Q and Xia J P 2016 *Appl. Phys. A* **122** 328

[37] Sun H X, Zhang S Y and Yuan S Q 2016 *Chin. Phys. B* **25** 124313

[38] Bhattacharya M C, Guy R W and Crocker M J 1971 *J. Sound Vib.* **18** 157

[39] Hou B, Mei J, Ke M Z, Liu Z Y, Shi J and Wen W J 2008 *J. Appl. Phys.* **104** 014909